CPQ Medicine (2018) 2:1
Research Article

Eletrochemiluminescence, Quantum Chemical Calculation, Electrochemical Impedance Spectroscopy, Electrochemical Potentiodynamic Polarization Study on the Corrosion Inhibition and Mechanism of Organic Inhibitors for Q235 Carbon Steel in 3.5% NaCl

Xuehui Pang*, Chunhuan Li, Xiaojian Li, Baocun Zhu, Jian Gao, Qin Wei & Bin Du

Key Laboratory of Chemical Sensing & Analysis in Universities of Shandong, School of Chemistry and Chemical Engineering, University of Jinan, Jinan 250022, P. R. China

***Correspondence to:** Dr. Xuehui Pang, Key Laboratory of Chemical Sensing & Analysis in Universities of Shandong, School of Chemistry and Chemical Engineering, University of Jinan, Jinan 250022, P. R. China.

Copyright

Received: 29 May 2018

Published: 10 July 2018

Keywords: *Corrosion Inhibition; Electrochemiluminescence; Quantum Chemical Calculation; Eis; Potentiodynamic Polarization*

Abstract

In this work, two kinds of corrosion inhibitor, 3',6'-dihydroxy-3H-spiro[isobenzofuran-1,9'-xanthen]-3-one DS and 8-Oxo-8H-acenaphtho [1, 2-b] pyrrole-9-carbonitrile AC, for Q235 carbon steel were studied by eletrochemiluminescence (ECL), quantum chemical calculation by Gaussian03W, electrochemical impedance spectroscopy (EIS), electrochemical potentiodynamic polarization test in 3.5% NaCl. ECL data both showed that the inhibitors emitted weaker luminescence on the carbon steel electrode (CSE) than the case on the glassy carbon electrode (GCE), and the emitted luminescence weakened more for DS than that for AC. ECL method was initially applied. The ECL results were illuminated by the quantum calculation data from

the aspect of the energy band. The interaction mechanism between the inhibitors and Fe atoms was illustrated by the quantum chemical calculation data. The EIS data showed that the inhibitors hindered more than 99% charger and mass transmission, R_p decreased and C_{dl} increased. The potentiodynamic polarization data showed that the inhibitors reduced most of the electrode reaction current j_{corr} and suppressed the anodic reaction more obviously. Thermomechanical analysis showed that the inhibitors behavior fitted well with Langmuir adsorption isotherm and the interaction strength fell in between the physical and chemical interaction.

Introduction

Many public facilities (communication facilities, power supply facilities, etc.), the industrial facilities (the drilling platform, the work platform in some harbor, etc.) and other important facilities are constructed with the carbon steel in the seawater generally. The inconspicuous and continuous corrosion of these carbon steel and metal equipments may lead to a sudden large disaster if no corrosion protection measures and equipments, resulting in serious economic losses and waste of materials. In order to prevent the corrosion of the metal equipments effectively, the corrosion inhibitors with excellent performance may be used in some certain cases, and the organic inhibitors are focused and more commonly used at present [1-5].

There are a lot of detection technologies and research methods for the evaluation of corrosion inhibitor performance recently, including weight loss method, electrochemical method (electrochemical impedance spectroscopy (EIS) [6-15] and potentiodynamic polarization [6-17], cyclic voltammetry [9,18,19], etc), spectroscopy method(surface enhanced Raman spectroscopy (SERS)[17,20], Infrared-visible sum frequency generation spectroscopy[3,12,21,22], XPS[23], etc.), and morphology method(SEM[19,24-28], TEM[25,29,30], AFM[31], etc). Some of the above methods are converted from other research fields. However, the traditional methods were facing with some problems such as the test course of the weight loss method was so long, the morphology method couldn't give the corrosion mechanism. Here we introduced the electrochemiluminescence (ECL), which was usually used in the biosensor field, to research the inhibition effect of the inhibitors and explain the interaction mechanism between the organic inhibitors and the carbon steel surface. ECL, which is also called electro-generated chemiluminescence, is electron transfer reaction on the vicinity of an electrode by combining electrochemistry with chemiluminescence. Due to advantages of low cost, high sensitivity, and wide application for various analytes, ECL has become a very powerful analytical technique in the areas of chemistry, nanomaterial, immunoassay, DNA detection, food and water testing, and biowarfare agent detection [29,32-38]. Especially, lots of corrosion inhibitors have the potential possibility to produce the luminescence. Then based on this property of the corrosion inhibitors, we realized the study of the corrosion inhibition effect using ECL method and further presented its mechanism which was expected to provide some valuable data and results.

The structure of organic corrosion inhibitor has a decisive influence on its corrosion inhibition performance, there is great significance and also some theoretical methods to research the relationship between the structure of organic corrosion inhibitor and the corrosion inhibition performance. Since the early 1970s, some scientists have been attempted to study the dependence of corrosion inhibitor properties and quantum

chemical parameters by some semi-empirical calculation method (AM1, PM3, zindo, etc.) and some quantum calculation method (Gaussion [39-44], molecular dynamic (MD) simulations [13,22,45,46], etc.). We attempted the density functional theory (DFT) methods by Gaussion 03 to explain ECL data, EIS data andpotentiodynamic polarization data, the phenomenon and the corrosion mechanism in microlevel.

So, the corrosion inhibition and mechanism of DS and AC (Fig. A. 1) for Q235 carbon steel were studied by ECL, quantum chemical calculation, EIS and electrochemical potentiodynamic polarization in 3.5% NaCl. ECL test perfectly researched the corrosion inhibition behaviour of the inhibitors and the way the inhibitors interacted with Fe atoms on Q235 carbon steel. Quantum chemical calculations were carried out to find the parameters, the optimized molecular structure, the electron density and the orbital density distribution of the frontier molecular orbital of the ground state and the excited state. And the interaction mechanism was found out by quantum chemical calculation analysis. EIS and electrochemical potentiodynamic polarization test were carried out to find out the corrosion inhibition effect and analyze the inhibition mechanism between the solid-liquid interfaces. The thermomechanical behavior of the inhibitors was also studied.

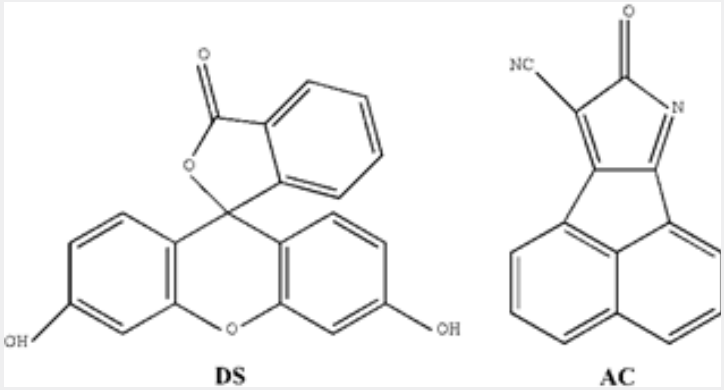

Figure A. 1: *Molecular structures of the inhibitors.*

Experimental

Materials

DS was purchased from sigma Aldrich Co. Ltd. (U.S.A), and AC was synthesized according to literature[47], ^{1}HNMR and ^{13}C NMR of AC was shown in Fig. A. 2 as follow: ^{1}H-NMR (400 MHz, DMSO-d_6) δ (*10^{-6}): 7.971(t, J = 7.6 Hz, 1H), 8.058(t, J = 7.6 Hz, 1H), 8.399(s, 1H), 8.642-8.696(m, 3H). ^{13}C-NMR (100 MHz, $CDCl_3$) δ (*10^{-6}): 113.371, 113.872, 119.657, 122.163, 126.030, 127.291, 127.900, 128.863, 131.312, 131.722, 132.634, 134.334, 137.625, 138.178, 177.45.

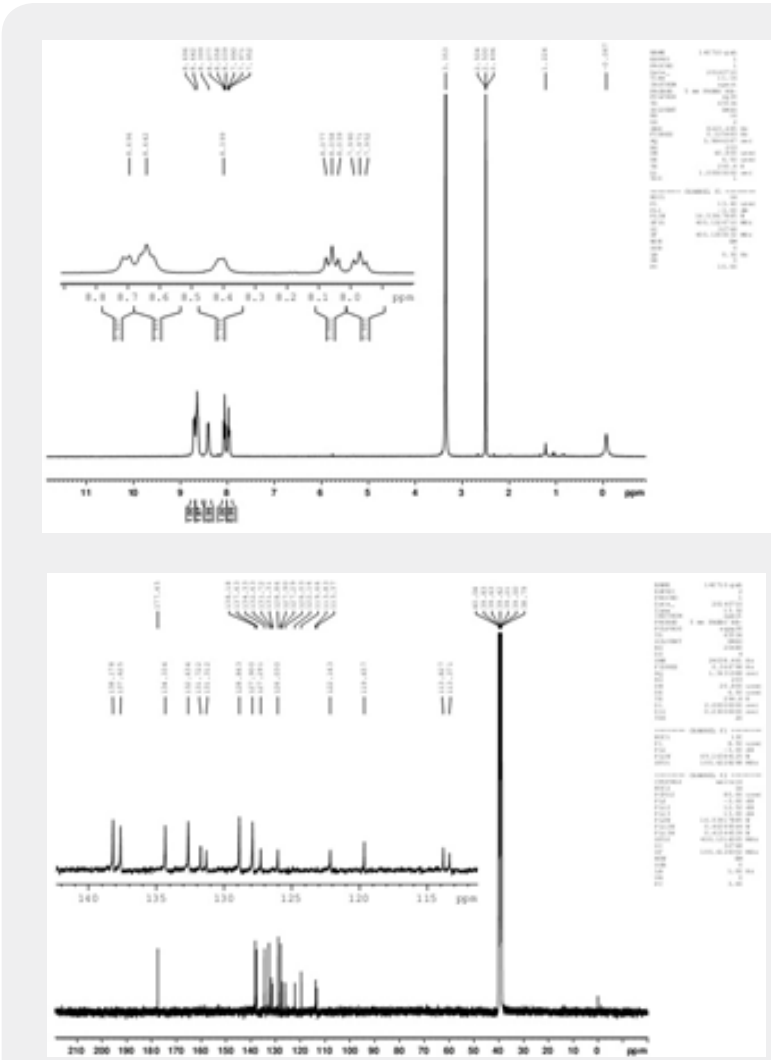

Figure A. 2: [1]HNMR and [13]CNMR of AC

Q235 carbon steel (Ø 0.4mm×40mm) only exposed cylindrical surface (Ø 0.4mm) into the electrolyte solution and the rest was covered by epoxy resin. The working Q235 carbon steel electrode (CSE) was polished smoothly using 180, 600, 1000, 2000 sandpaper and WAW5 (06) metallographic sandpaper in sequence, rinsed with ultra-pure water from UPT-I-10/20T ultra-pure water equipment (Chengdu Ultrapure Technology Co. Ltd., China) and dried for use at 298K.

The glassy carbon electrode (GCE) was polished with 0.05mm Al_2O_3 powder on a polishing pad, rinsed with ultra-pure water and dried for use at 298 K.

The working solutions added the inhibitors of 10^{-3}mol dm^{-3}, 10^{-4}mol dm^{-3}, 10^{-5}mol dm^{-3}, 10^{-6}mol dm^{-3}, 10^{-7} mol dm^{-3} respectively were prepared. 3.5% NaCl solution was used as blank control. The working solution and the blank solution were dropped on the working electrode and the inhibitors self-assembled on the electrode surface for 2h.

A traditional three-electrode system was used in all experiments. The platinum electrode was the auxiliary electrode, CSE and GCE were the working electrodes. All experiments were controlled at 298K.

ECL Experiment

The ECL experiments were carried out on a BPCL-1(-T-G-C) Urtra Weak Chemiluminescence Analyzer (Institute of Biophysics, Chinese Academy of Sciences, China) and cyclic voltammetry (CV) tests were carried out on a CHI760D electrochemical workstation (Chenhua Instrument Shanghai Co. Ltd., China) using an Ag/AgCl electrode as reference electrode at the same time. The potential scanned from -2.0V to +0.5V at the scan rate 0.1V/s.

Electrochemical Impedance Spectroscopy (EIS)

EIS experiments were carried out on a IM6ex Electrochemical workstation (ZAHNER, German) using a saturated calomel electrode (SCE) as the reference electrode. The frequency ranges from 10mHz to 100kHz, the amplitude was 5mV ac signal. The parameters of EIS were obtained using SIM software.

Potentiodynamic Polarization Test

The potentiodynamic polarization curves (Tafel curves) were obtained from CHI760D Electrochemical (Chenhua Instrument Shanghai Co., Ltd., China) workstation using an Ag/AgCl electrode as reference electrode by changing the electrode potential automatically from -0.6V to +0.5V (vs. Ag/AgCl) with a scan rate of 0.5mV/s.

Quantum Chemical Calculations

All of the calculations were carried out with Gaussian03W on a sugon I620-G10 server (Sugon Information Industry Co., ltd., China). For the ground states, the calculations were carried out with DFT by B3LYP method using 6-311G basis set. For the excited states, the calculations were carried out with time dependent density functional theory (TD-DFT) by B3LYP method using 6−311++G (3DF, 3pd) basis set.

Results and Discussion

ECT Results

In order to reveal that the corrosion inhibition behavior of both inhibitors, whether and how the inhibitors interacted with Q235 carbon steel surface, the ECL experiments were carried out as shown in Fig.3. It can be seen that both of the inhibitors show the luminescence signal, and the ECL intensity of the inhibitors on the GCE and the CSE enhanced with the increasing concentration of the corrosion inhibitors. ECL intensity showed positive correlations with the inhibitors concentration. There was no ECL intensity extreme value for both inhibitors whether on the GCE or on the CSE. But in consideration that the corrosion inhibitors need good inhibition effect within much lower concentration, ECL test toward lower concentration are researched emphatically. At the same time, we used the ECL test on the GCE as the reference so that the interaction between the CSE and the inhibitors can be studied.

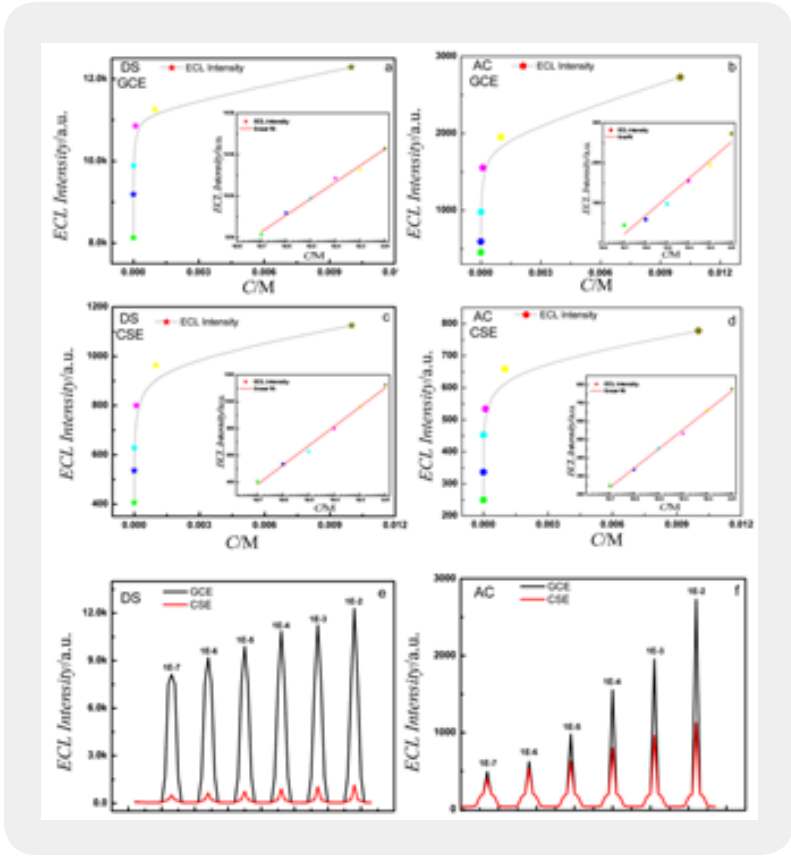

Figure A. 3. *The relationship between ECL intensity of GCE and CSE and two kinds of inhibitor concentration without and with different concentrations of corrosion inhibitor at 298 K*

Firstly, from Fig.3 a~d, we could find that whether using DA or AC, the ECL intensity on the GCE was higher than that on the CSE at the same concentration, and this intensity difference depended on the internal chemical quality of the inhibitors. And secondly, it can be seen from Fig.3 e~f more obviously, the ECL intensity of AC was not strong as the case of DS whether on the CSE or on the GCE, which meant the different interaction intensity between the electrode and the inhibitors must exist. Thirdly, under the same concentration, the ECL intensity of DS on the GCE was higher than that on the CSE, so in the same case of AC, and this situation showed that the interaction mechanism between the electrode and the inhibitors was the same. So, why the interaction intensity between the different electrode and the inhibitors changed at different level? What's the interaction mechanism between the electrode and the inhibitors? The following explanation might answer the both questions:

We know that the luminescence showed in the ECL test was one kind of the energy pattern. The luminescence occured when the energy release from the substances excite state to its ground state, and the excite state was generated by the electric current in the ECL test. The released energy of different substance was of different amount, then the intensity of the emitted luminescence was different inevitably even under the same condition. In this work the above mentioned problem can be described as in Fig.A3 and Fig.A4. It can be seen that the intensity of the emitted luminescence of the two inhibitors was obviously different even on

the same electrode at the same concentration, and the difference depended on the initial quality of the substance. For the same substance, the intensity of the emitted luminescence was obviously different on the GCE and on the CSE, which suggested that the emitting mechanism of the luminescence was different. But the intensity of the specific substance on the specific electrode at the same test situation should be the same, then we used the ECL intensity on the GCE as reference and took the energy released from the excite state to its ground state as the whole. It can be seen that at the same concentration, such as DS, the intensity on the CSE was weaker than that on the GCE and this phenomenon was more serious with the increasing concentration, which meant that the energy released from DS's excite state to its ground state occurred transfer on the CSE surface. A fraction of the energy missed, so did in the case of AC, but where to miss? All of the test situations were the same except the electrode in all of the experiments, so the disappeared energy must be transferred to the CSE, which meant DS molecules interacted with Fe atoms on the CSE surface. The more energy transferred, the stronger interaction occurred. While less energy used to luminesce, AC was in the same case. The above discussions explained the following questions: the reason why the interaction intensity between the different electrode and the inhibitors changed was both the initial quality of the inhibitors and the electrodes were different. It explained the interaction mechanism between the electrode and the inhibitors was because some energy transferred from the inhibitor to the CSE.

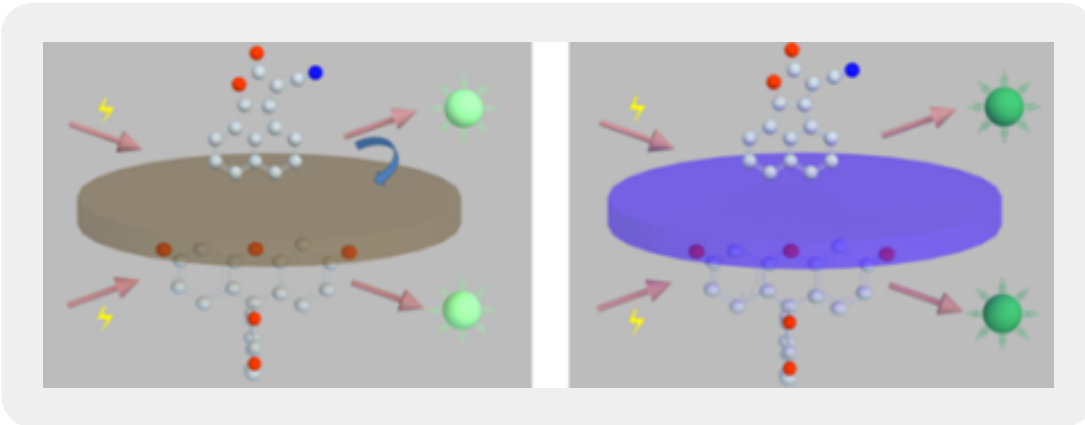

Figure A. 4: *The schematic diagram for ECL mechanism of the inhibitors (left for the inhibitors on CSE, right for inhibitors on GCE)*

AC; DS (the grey atoms for C, the blue atoms for N, the red atoms for O); CSE; GCE; electric current; the emitting light with different intensity

At the same concentration, the intensity of DS weakened more than that of AC, which meant the interaction between the CSE and DS was stronger than that between the CSE and AC. For example, at concentration of 10^{-7}mol dm^{-3}, the weakened intensity of DS was 7612 a.u., but that of AC was only 86 a.u., the same case could be found at 10^{-2}mol dm^{-3}, the weakened intensity of DS was 11135 a.u., for AC was only 1604 a.u. And we know the inhibitor behaved the corrosion inhibition effect for the carbon steel through the interaction between Fe atom and the inhibitor [24,41,44,46,48], so the above phenomenon announced DS and AC both showed the corrosion inhibition effect and DS acted better corrosion inhibition than AC.

From the above results, we can deduce that ECL was a feasible and optional method for the detection of the corrosion inhibition, especially for the substance which can emit the luminescence, such as the dye [49-52], the fluorescein [47,53-55]. But how the interaction between the CSE and the inhibitor occurred in the quantitative micro world, namely the interaction mechanism, the explanation will be showed in quantitative chemical calculation discussion.

Quantum Chemical Calculation

By the calculations, 3D molecular structure of the ground state and the excited state were obtained, the electron density distribution of the highest occupied molecular orbital (HOMO) of the ground state and the excited state, the energy level of HOMO of the ground state and the excited state, the orbital density distribution of the lowest unoccupied molecular orbital (LUMO) of the ground state and the excited state, the energy level of LUMO of the ground state and the excited state, the energy level difference between HOMO and LUMO, respectively.

Theoretical calculations provided a molecular-level explanation of the observed experimental behavior. The optimized geometry of the inhibitors was shown in Fig.5. A for the ground state and in Fig.5B for the excited state. It can be seen the structure of the inhibitors did not change from the ground state to the excited state. AC could interact with steel surface to the largest extent if AC molecules were self-assembled on the CSE at nearly 0° contact angle, but it has worse inhibitory efficiency than DS, which might be influenced by the electron density on HOMO and the orbital density on LUMO as the following explanation although AC has approximately planar structure.

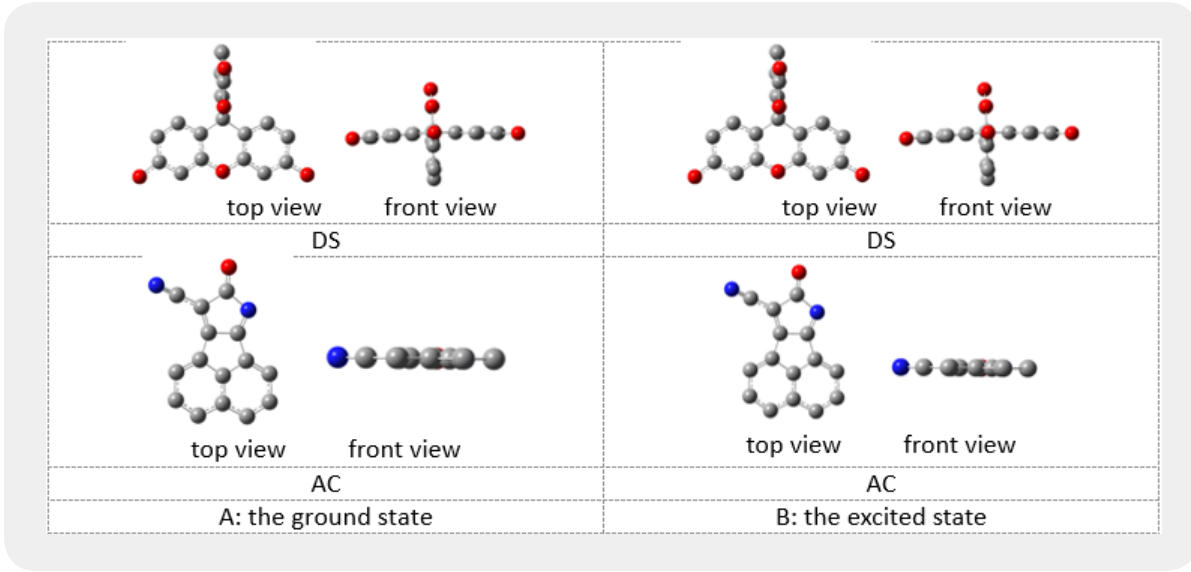

Figure A. 5: *Optimized geometry for inhibitors and (The blue are N atoms, the red are O atoms and the grey are C atoms)*

In order to obtain more details, the highest and the lowest value of the two spin degeneracy orbital were mapped at the isovalue 0.07 and were shown in Fig. 6A for the ground state and in Fig. 6B for the excited state.

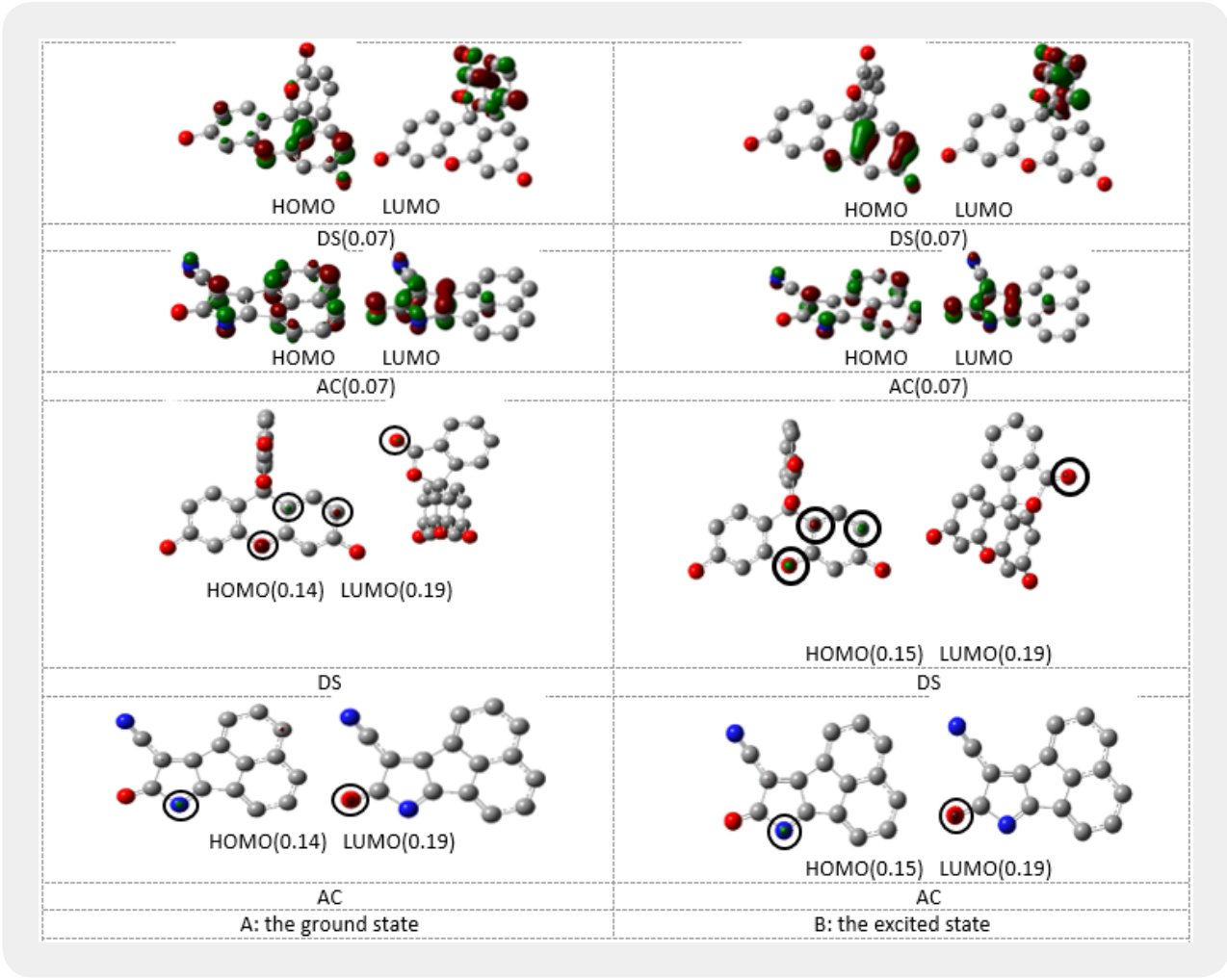

Figure A. 6: *The frontier molecule orbital density distribution for the excited state(The blue are N atoms, the red are O atoms and the grey are C atoms)*

The electron configuration of Fe atom was [Ar] $4s^2 3d^6$. The unfilled 3d orbital could accept the electron from the inhibitors and could bond with HOMO [24] of the inhibitors, while the filled 4s orbital could donate the electron to LUMO of the inhibitors and could bond with LUMO. So it can be predicted that some part of the interaction (the chemical interaction) of inhibitors on the metal surface may be ascribed to the interaction between 3d, 4s orbital of Fe atom and the front molecular orbital of the inhibitors [56].

In case of the LUMO (isovalue = 0.07) (Fig.6), four benzoic acid lactones of DS and Oxa-carbonitrile-pyrrole of AC had strong orbital density distributions both on the ground state and on the excited state. And the orbital density distribution of DS was stronger than that of AC, which indicated that DS had stronger

ability to accept preferentially the electron from 4s orbital of Fe [57]. For DS, the orbital density distributions of benzoic acid lactones of the excited state were stronger than that of the ground state. But for AC, the orbital density distributions of Oxa-carbonitrile-pyrrole of the excited state was weaker than that of the ground state, which would result in the ability to interaction with Fe atoms of DS was stronger than that of AC.

In case of the HOMO (Fig.6) (isovalue = 0.07), the electron density on oxa-anthracene and adjacent hydroxy of the ground state, one benzene cycle of oxa-anthracene and two adjacent hydroxy of the excited state for DS had larger electron distribution density. And the electron density on two benzene cycles of acenaphthene ring, N atoms of –CN and pyrrole cycle had the larger distribution density of the ground state and the excited state for AC. For DS, the electron density of two benzene cycle of oxa-anthracene and two adjacent hydroxyl of the excited state was stronger than that of the ground state; the other benzene cycle of oxa-anthracene of the excited state almost showed nothing. But for AC, the orbital density distributions of two benzene cycles of acenaphthene ring, N atoms of -CN and pyrrole cycle of the excited state was weaker than that of the ground state, which would decrease the feasibility to bind with 3d orbital of Fe atoms.

In order to prove the above mentioned results about the frontier molecule orbital, we mapped residual HOMO at the isovalue 0.14 for the ground state and at 0.15 for the excited state as shown in Fig.6. It can be seen that the electron density distribution of the excited state was higher than that of the ground state whether for DS or for AC. And the residual electron density distribution on HOMO of DS still existed and was higher than that of AC even at high isovalue 0.16 for the ground state and the excited state, which indicated that HOMO of DS showed more powerful ability to interact with 3d orbital of Fe atoms. And also there was the positive correlation between the electron density distribution of HOMO and the inhibitory efficiency as had been reported earlier [48,58]. And also, we mapped residual LUMO at the isovalue 0.19 for the ground state and the excited state as shown in Fig.6. It can be seen that the orbital density distributions on LUMO of the excited state and of the ground state was almost same for DS and for AC. The residual orbital density distributions on LUMO lost at 0.19 for the ground state and lost at 0.21 for the excited state for them. And there was no positive correlation between the orbital density distributions of LUMO and the inhibitory efficiency as had been reported earlier [48,59]. There were three acting sites for DS but one for AC on HOMO whether for the ground state or for the excited state until the electron density distribution lost at 0.22. And this kind of case was not obvious for the orbital density distributions of LUMO whether for the ground state or for the excited state, which indicated that DS had the better interaction ability with Fe atom and may show the better corrosion inhibition effect.

And we can find out how the energy transferred between the inhibitors and Fe atom of Q235 carbon steel electrode by energy band matching by the quantum chemistry calculation. We know that the work function φ of Fe is 4.500eV, and the work function can be deduced by Evol (the energy zero in vacuum) and EFi (the Fermi energy of Fe) as the following equation:

$$\varphi = E_{vol} - E_{Fi}$$

So, it can be deduced that E_{Fi} is -4.500eV. And also, the energy level of the LUMO and HOMO of the inhibitors were shown in order of energy level in Fig.7, we can see that the energy level of the LUMO and HOMO of the excited state was higher than those of the ground state whether for DS or for AC, which suggested that the inhibitors adsorbed the energy from the electrode. And we can see that the energy level of HOMO and LUMO of the excited state for AC was respectively -6.667eV, -3.673eV, and the energy level of HOMO and LUMO of the excited state for DS was -5.714eV and -1.524eV respectively. All of the calculated energy level by Gaussion were relative to the energy zero in vacuum [60].

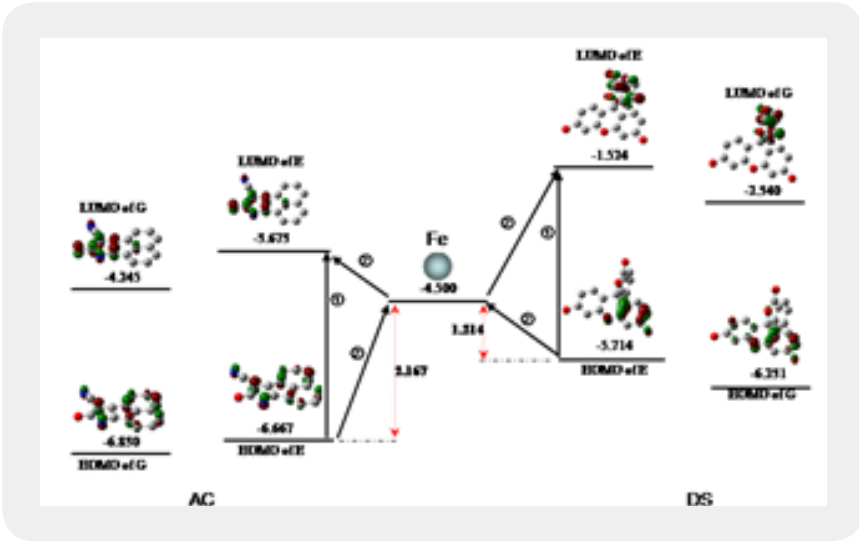

Figure A. 7: *The energy level (eV) and the transition way of the inhibitors of the ground state (G) and the excited state (E)*

We know that the emitted luminescence was produced by the energy from the course of the electron in the LUMO jumped from the HOMO in general as described route ① in Fig.7. But on the CSE due to E_{Fi} of Fe was between the energy level of LUMO and the HOMO of both inhibitors, it can be deduced the emitted route of luminescence might change partially as described route ② as mentioned in some articles about the photoelectric material [28,34,35,61], And also the effect of this course was similar to the PET process [62-64]. So, when a portion of electrons jumped from the HOMO of the inhibitors would firstly jump to the 3d orbital of Fe but not to the LUMO of the inhibitors. We know the electron configuration of Fe atom was [Ar] $4s^2 3d^6$, the unsaturated 3d orbital of Fe atom can accept the electron from the inhibitors and the energy level of 3d orbital was lower than the LUMO of the inhibitors, resulting in electrons stay. This course illuminated that why the ECL intensity of the inhibitors on GCE was higher than that on the CSE and how the energy transferred, namely what's the interaction mechanism between the electrode and the inhibitors.

The energy level of HOMO of the excited state of AC and DS was respective -6.667eV and -5.714eV, then the energy gap between the energy level HOMO and EFi of Fe was respective 2.167eV and 1.214eV, so it can be deduced that it was easier for the electrons of DS to jump from the HOMO to the 3d orbital of Fe atom than the case of the electrons of AC because of much little energy gap. And this course explained

why the weakened intensity for DS was much larger than the case of AC and why the interaction intensity between the different electrode and the inhibitors changed at different level.

EIS Results

The corrosion behavior of the CSE in the blank solution and in the working solution was studied at 298K. The Nyquist plots were shown in Fig.8. The figure showed that impedance spectra were similar in a single but not perfect loop [65]. The semicircle diameter illustrated the charge transfer resistance and indicated the behavior of the redox couple on the electrode surface. The deviations from an ideal semicircle were generally attributed to frequency dispersion, the inhomogeneities in the surface and the mass-transport resistance, therefore the Nyquist plots can be used as a signal to characterize the self-assembly effect of the inhibitors. These electrochemical systems can be interpreted by the usual R_s-(R_p-C_{dl}) equivalent circuit in Fig.9 [66, 67]. C_{dl} values were obtained from Eq. (A.1):

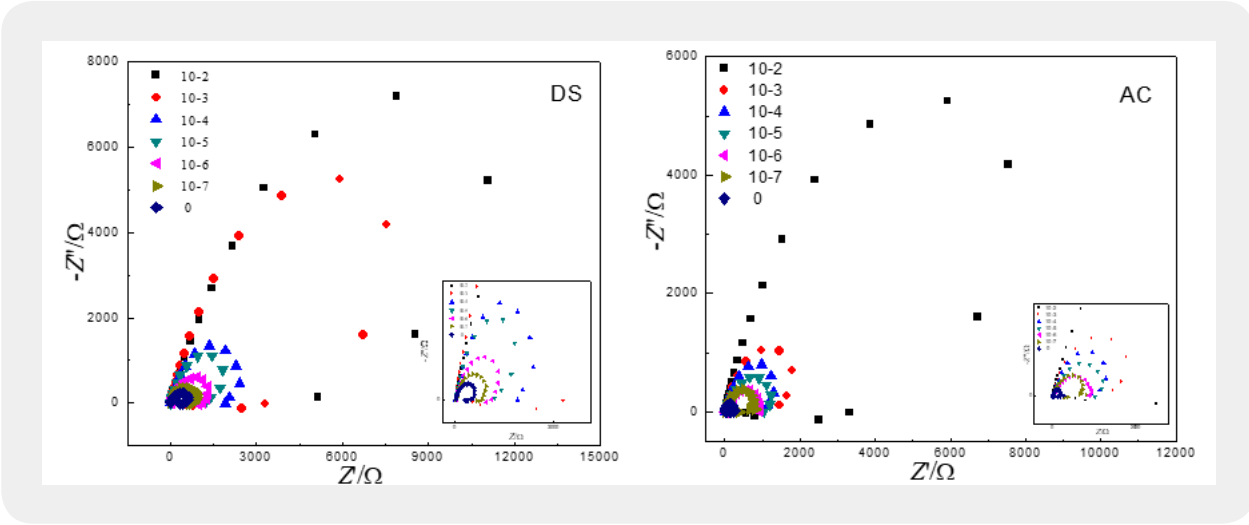

Figure A. 8: *Nyquist diagram for CSE in 3.5% NaCl for inhibitors at room temperature*

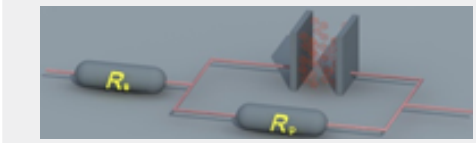

Figure A. 9: *R_s-R_p-C_{dl} Equivalent circuit model used to fit EIS data*

why the weakened intensity for DS was much larger than the case of AC and why the interaction intensity between the different electrode and the inhibitors changed at different level.

All the impedance parameters were given in Table 1 (R_p and C_{dl} values were adjusted concerning the working electrode area exposed to the solution). It can be seen that the two compounds did show obvious inhibition effect at 10^{-7} mol dm^{-3}. The inhibitory efficiency IE% increased obviously with the increasing concentration, and markedly increased reaching the highest value 99.99% (DS), 99.99% (AC) at 10^{-2}mol dm^{-3}, especially in the case of DS. And also R_p increased with the increasing concentration, reaching the highest value $3.927\times10^{9}\Omega$ cm^{-2} (DS), 1.759×109 Ω cm^{-2} (AC). C_{dl} tended to decrease, reaching the lowest value 9.150×10^{-13}Fcm^{-2} (DS), 3.328×10^{-10} F cm^{-2} (AC) at 10^{-2}mol dm^{-3}. C_{dl} decrease ($C_{dl}=\varepsilon/4\pi d$) might result from the displacement of the H2O molecules by the inhibitor molecules because H_2O molecules had higher dielectric constant but the inhibitor molecules had lower dielectric constant at the interface of the electrical double layer. which suggested that the two inhibitor molecules had been functioned at the metal-solution interface [68]. So the charge transfers between the solution and the metal surface had been inhibited sharply. R_p increase indicated that the corrosion resistance from the thickness increase of the compact self-assemble inhibitors film on the metal surface increased obviously, especially at the maximum concentration. It meant the inhibitors prevented the mass and charge transferred through the electrical double layer, therefore the corrosion rate also decreased rapidly. It can be deduced DS and AC showed excellent inhibitory effect, but DS showed the lower C_{dl} and the higher R_p, which indicated DS behaved better inhibition effect as ECL and quantum chemical calculation suggested.

Table. 1. *Impedance parameters in 3.5% NaCl at 298K*

	***c*/mol dm^{-3}**	***R_p*/Ω cm^{-2}**	***C_{dl}*/F cm^{-2}**	***IE*/ %**
blank	0	2.727×10^{3}	6.113×10^{-4}	
DS	10^{-7}	4.869	3.424×10^{-4}	43.99
	10^{-6}	6.187	1.5822×10^{-4}	55.92
	10^{-5}	8.960×10^{3}	3.980×10^{-5}	69.56
	10^{-4}	1.091×10^{4}	5.465×10^{-6}	75.00
	10^{-3}	1.504×10^{4}	3.891×10^{-9}	81.87
	10^{-2}	3.927×10^{9}	9.150×10^{-13}	99.99
AC	10^{-7}	6.140×10^{3}	1.594×10^{-4}	55.59
	10^{-6}	9.223×10^{3}	6.346×10^{-5}	70.43
	10^{-5}	1.510×10^{4}	9.297×10^{-6}	81.94
	10^{-4}	1.956×10^{4}	4.635×10^{-6}	86.06
	10^{-3}	4.111×10^{4}	7.017×10^{-8}	93.37
	10^{-2}	1.759×10^{9}	3.328×10^{-10}	99.99

$$IE = \frac{R_p - R_{p,blank}}{R_p} \times 100$$

Potentiodynamic Polarization Measurements

Fig.10 showed polarization curves for Q235 carbon steel in blank control solution and the working solutions. Electrochemical corrosion kinetic parameters obtained by extrapolation of Tafel lines were given in Table 2. From Fig.10, it can be seen that the cathodic and anodic current-potential curves gave rise to nearly parallel Tafel lines, which suggested the hydrogen-evolution reaction on the cathode and the iron-dissolution reaction on the anode were activation-controlled. The addition of the two inhibitors did not modify the electrode electrochemical reaction mechanism.

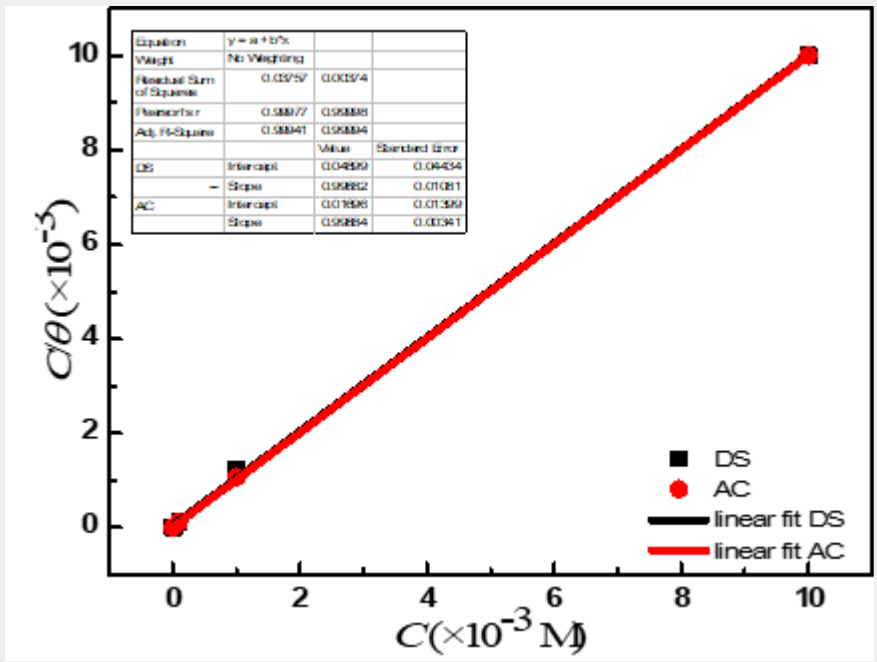

Figure A. 10: *Langmuir interaction isotherm for inhibitors on CSE in 3.5% NaCl at 298K*

Table 2: *Polarization Parameters in 3.5% NaCl at 298 K*

	c/mol dm^{-3}	*E*/mV	j_{corr}/μAcm^{-2}	β_a/mV dec^{-1}	β_c/mV dec^{-1}	*IE*/%
blank		413	823	52	41	—
DS	1.0×10^{-7}	346	273	62	53	67
	1.0×10^{-6}	312	234	81	60	72
	1.0×10^{-5}	299	158	84	65	81
	1.0×10^{-4}	199	107	87	73	87
	1.0×10^{-3}	136	82	130	96	90
	1.0×10^{-2}	94	45	148	103	95
AC	1.0×10^{-7}	352	371	23	43	55
	1.0×10^{-6}	323	312	41	54	62
	1.0×10^{-5}	307	253	68	62	69
	1.0×10^{-4}	212	190	80	79	77
	1.0×10^{-3}	123	154	112	87	81
	1.0×10^{-2}	85	100	130	93	88

$$IE\% = \frac{j^{\circ}_{corr} - j_{corr}}{j^{\circ}_{corr}} \times 100$$

From Fig.10 and Table 2, it can be seen that the values of anodic slope (β_c) were modified slightly and those of cathodic slope (β_a) changed markedly with the increased working concentration of the inhibitors. The slightly changed β_c clearly indicated that the addition of the inhibitors did not change the kinetics of cathodic proton–discharge reaction obviously. But the markedly changed β_a indicated the anodic iron dissolution was influenced obviously.

We know that the relationship between E and lg*I* can be described in the strong polarization region by Tafel Eq. (A.2), β is the slope of Tafel linear region of the Tafel polarization curve, and can be calculated by Eq. (A.3). From Eq. (A.3), it can be seen that within the same △E, △(lg*I*) changed more less, the value of β got bigger, the corrosion inhibition effect got better, the polarization curve went up more slowly along the direction, the polarization curve looked almost like a platform and even *I* changed lower as showed in Fig.10. And the platform got more horizontal, the corrosion inhibition effect performed better. So we can see from Fig.10 that the curve of DS showed much better inhibition effect but the curve of AC showed unconspicuous inhibition effect. And it can also be induced from Table. 2, the modification extent of β_c and β_a of DS was greater, which explained why the addition of DS considerably reduced the cathodic and anodic current densities, and also showed markedly the better inhibitory efficiency. β_a was higher than β_c whether

When the potential was more positive than -310mV (DS), the dissolution of the metal ion of the Q235 carbon steel increased obviously and the inhibitors adsorbed more difficultly. The polarization curves extended to the same direction, which showed that there was no effective inhibitory effect. It might be that the inhibitors left from the electrode surface and could not prevent the large mass-transfer led by electrode reaction.

Fig.10 and Table 2 showed that the current density values of both cathodic current density (i_k) and anodic current density (i_a) decreased in the working solution comparing with those in the blank solution. And total current density j_{corr} reached their lowest values, 45μA cm^{-2} (DS), 100μA cm^{-2} (AC). So, it can be deduced that there existed the inhibition ability in the order of DS > AC.

Thermomechanical Analysis

In order to understand the mechanism of corrosion inhibition well, the thermodynamic adsorption behavior of DS and AC on the CSE surface was studied. Because the charge–transfer resistance was related to the coverage of the inhibition molecule on the CSE surface, the degree of surface coverage θ was equal to *IE%* in values here. To determine the interaction model and its kinetics parameter interaction equilibrium constant K, various isotherms were tested. The Langmuir one [69] was the best obtained straight line fit well with Eq. (A.4).

Fig.11 showed that the C and C/θ had good linear relationship with correlation coefficients of 0.99977 (DS), 0.99998 (AC), which confirmed the interaction behavior of the two inhibitors on the CSE surface in 3.5% NaCl followed Langmuir interaction isotherm perfectly. The interaction equilibrium constant K values of DS and AC were 4.55×10^5, 1.77×10^6 respectively, indicating strong interaction between the inhibitor and Fe atom in 3.5% NaCl. The interaction equilibrium constant *K* was calculated by Eq. (A.5).

$\triangle G_m$ for DS and AC were both negative values, -34.5kJ/mol and -37.2kJ/mol respectively, which suggested that the inhibitors could spontaneously self-assemble on the CSE surface at 298 K. According to thermodynamics, $\triangle G_m$ values higher than -20kJ/mol involve physical interaction associated with an electrostatic interaction between charged molecules and the charged metal surface; $\triangle G_m$ values lower than -40kJ/mol involve chemical interaction based on charge share or transference through the chemical bonds formation [70]. The values of $\triangle G_m$ for DS and AC were both slightly higher than -40kJ/mol, and it indicated that the interaction of two inhibitors on metal surface in 3.5% NaCl was the mixed result of physical interaction and chemical interaction, but the latter mainly acted.

Conclusions

In this work, two organic compounds acted as corrosion inhibitor for Q235 carbon steel, all of the results of ECL data, quantum chemical calculations, EIS data, potentiodynamic polarization data showed that both of the inhibitors behaved good corrosion inhibition effect and DS showed better protection effect than AC.

ECL data and the ECL work mechanism illuminated the interaction intensity and the interaction mechanism between Fe atoms and the inhibitors. ECL data showed that the interaction intensity between the different electrode and the inhibitors changed at different level. The results proved that ECL can be be applied to corrosion inhibition research.

Quantum chemical calculations analyzed the reason of the good corrosion inhibition effect by 3D structure, the energy level, the electron density and the orbital distribution of the frontier orbital. And also, the interaction mechanism was explained by the energy band structure both of the inhibitors and Fe atom and by the influence of the energy level of Fe atom on the electron jumping course from HOMO to LUMO of the inhibitors through DFT theory, EIS data, potentiodynamic polarization data showed They can block the vast majority of the reaction current, mass transmission and decreased the capacitance markedly through double electrode layer existed on the Q235 carbon steel surface.

Acknowledgments

This research was supported by National Natural Science Foundation of China (No. 21175057, 21375047, 21377046), Shandong Provincial Natural Science Foundation, China (No. ZR2011EMQ010), the Science and Technology Development Plan of Shandong Province (No. 2014GSF120004), and Qin Wei thanks the Special Foundation for Taishan Scholar Professorship of Shandong Province and UJN (No. ts20130937).

Appendices A

Eq.(A.1)

$$C_{dl} = \frac{1}{2\Pi f_{\max} R_p}$$

Eq.(A.2)

$$E = \mathrm{a} + \beta \lg I$$

Eq.(A.3)

$$\beta = \frac{\Delta E}{\Delta(\lg I)}$$

Eq.(A.4)

$$\frac{C}{\theta} = C + \frac{1}{K}$$

Eq.(A.5)

$$K = \exp\left(-\Delta G_m / RT\right) / 55.5$$

Appendices B

f_{max}: the frequency at which the imaginary component of the impedance was the maximum

C_{dl}: the double-layer capacitance

R_p, blank: the charge–transfer resistance in the presence of inhibitor

R_p: the charge–transfer resistance in the absence of inhibitor

I_{corr}^0 : the corrosion current density in absence of inhibitor

I_{corr} : the corrosion current density in presence of inhibitor

55.5: the molar concentration of water in the solution

$\triangle G_m$: the free energy of interaction

Bibliography

1. Kokalj, A., Peljhan, S., Finsgar, M. & Milosev, I. (2010). What Determines the Inhibition Effectiveness of ATA, BTAH, and BTAOH Corrosion Inhibitors on Copper? *Journal of the American Chemical Society, 132*(46), 16657-16668.

2. Weiss, S. & Reemtsma, T. (2005). Determination of benzotriazole corrosion inhibitors from aqueous environmental samples by liquid chromatography-electrospray ionization-tandem mass spectrometry. *Analytical Chemistry, 77*(22), 7415-7420.

3. Schultz, Z. D., Biggin, M. E., White, J. O. & Gewirth, A. A. (2004). Infrared-visible sum frequency generation investigation of Cu corrosion inhibition with benzotriazole. *Analytical Chemistry, 76*(3), 604-609.

4. Szunerits, S. & Walt, D. R. (2002). Aluminum surface corrosion and the mechanism of inhibitors using pH and metal ion selective imaging fiber bundles. *Analytical Chemistry, 74*(4), 886-894.

5. Thorpe, J. M., Beddoes, R. L., Collison, D., Garner, C. D., Helliwell, M., Holmes, J. M. & Tasker, P. A. (1999). Surface coordination chemistry: Corrosion inhibition by tetranuclear cluster formation of iron with salicylaldoxime. *Angewandte Chemie-International Edition, 38*(8), 1119-1121.

6. Loganayagi, C., Kamal, C. & Sethuraman, M. G. (2014). Opuntiol: An Active Principle of Opuntia elatior as an Eco-Friendly Inhibitor of Corrosion of Mild Steel in Acid Medium. *Acs Sustainable Chemistry & Engineering, 2*(4), 606-613.

7. Suedile, F., Robert, F., Roos, C. & Lebrini, M. (2014). Corrosion inhibition of zinc by Mansoa alliacea plant extract in sodium chloride media: Extraction, Characterization and Electrochemical Studies. *Electrochimica Acta., 133*, 631-638.

8. Babic-Samardzija, K., Lupu, C., Hackerman, N., Barron, A. R. & Luttge, A. (2005). Inhibitive properties and surface morphology of a group of heterocyclic diazoles as inhibitors for acidic iron corrosion. *Langmuir, 21*(26), 12187-12196.

9. Prasai, D., Tuberquia, J. C., Harl, R. R., Jennings, G. K. & Bolotin, K. I. (2012). Graphene: Corrosion-Inhibiting Coating. *ACS Nano., 6*(2), 1102-1108.

10. Hsieh, Y. P., Hofmann, M., Chang, K. W., Jhu, J. G., Li, Y. Y., Chen, K. Y., Yang, C. C., Chang, W. S. & Chen, L. C. (2013). Complete Corrosion Inhibition through Graphene Defect Passivation. *ACS Nano., 8*(1), 443-448.

11. Alvarez, F., Grillo, C., Schilardi, P., Rubert, A., Benítez, G., Lorente, C. & Fernández Lorenzo de Mele, M. (2012). Decrease in Cytotoxicity of Copper-Based Intrauterine Devices (IUD) Pretreated with 6-Mercaptopurine and Pterin as Biocompatible Corrosion Inhibitors. *ACS Applied Materials & Interfaces, 5*(2), 249-255.

12. Oguzie, E. E., Adindu, C. B., Enenebeaku, C. K., Ogukwe, C. E., Chidiebere, M. A. & Oguzie, K. L. (2012). Natural Products for Materials Protection: Mechanism of Corrosion Inhibition of Mild Steel by Acid Extracts of Piper guineense. *The Journal of Physical Chemistry C., 116*(25), 13603-13615.

13. Oguzie, E. E., Oguzie, K. L., Akalezi, C. O., Udeze, I. O., Ogbulie, J. N. & Njoku, V. O. (2012). Natural Products for Materials Protection: Corrosion and Microbial Growth Inhibition Using Capsicum frutescens Biomass Extracts. *Acs Sustainable Chemistry & Engineering, 1*(2), 214-225.

14. Pan, Y. C., Wen, Y., Xue, L. Y., Guo, X. Y. & Yang, H. F. (2012). Adsorption Behavior of Methimazole Monolayers on a Copper Surface and Its Corrosion Inhibition. *The Journal of Physical Chemistry C., 116*(5), 3532-3538.

15. Dandia, A., Gupta, S. L., Singh, P. & Quraishi, M. A. (2013). Ultrasound-Assisted Synthesis of Pyrazolo[3,4-b]pyridines as Potential Corrosion Inhibitors for Mild Steel in 1.0 M HCl. *Acs Sustainable Chemistry & Engineering, 1*(10), 1303-1310.

16. Duda, Y., Govea-Rueda, R., Galicia, M., Beltran, H. I. & Zamudio-Rivera, L. S. (2005). Corrosion inhibitors: Design, performance, and computer simulations. *Journal of Physical Chemistry B., 109*(47), 22674-22684.

17. Cao, P. G., Gu, R. N. & Tian, Z. Q. (2002). Electrochemical and surface-enhanced Raman spectroscopy studies on inhibition of iron corrosion by benzotriazole. *Langmuir, 18*(20), 7609-7615.

18. Cabrini, M., Lorenzi, S. & Pastore, T. (2014). Cyclic voltammetry evaluation of inhibitors for localised corrosion in alkaline solutions. *Electrochimica Acta., 124*, 156-164.

19. Wang, Y. H. & He, J. B. (2012). Corrosion inhibition of copper by sodium phytate in NaOH solution: Cyclic voltabsorptometry for in situ monitoring of soluble corrosion products. *Electrochimica Acta., 66*, 45-51.

20. Shen, S., Zhu, C. d., Guo, X. y., Li, C. c., Wen, Y. & Yang, H. F. (2014). The synergistic mechanism of phytic acid monolayers and iodide ions for inhibition of copper corrosion in acidic media. *RSC Advances, 4,* 10597-10606.

21. Roy, A., Pal & Sukul, D. (2014). Origin of the synergistic effect between polysaccharide and thiourea towards adsorption and corrosion inhibition for mild steel in sulphuric acid. *RSC Advances, 4,* 10607-10613.

22. Feng, L., Yang, H. & Wang, F. (2011). Experimental and theoretical studies for corrosion inhibition of carbon steel by imidazoline derivative in 5% NaCl saturated Ca(OH)2 solution. *Electrochimica Acta., 58,* 427-436.

23. López, D. A., Schreiner, W. H., de Sánchez, S. R. & Simison, S. N. (2003). The influence of carbon steel microstructure on corrosion layers: An XPS and SEM characterization. *Applied Surface Science, 207*(1-4), 69-85.

24. Zhao, P., Liang, Q. & Li, Y. (2005). Electrochemical, SEM/EDS and quantum chemical study of phthalocyanines as corrosion inhibitors for mild steel in 1mol/l HCl. *Applied Surface Science, 252*(5), 1596-1607.

25. Zhang, L., Niu, W., Gao, W., Qi, L., Lai, J., Zhao, J. & Xu, G. (2014). Synthesis of Convex Hexoctahedral Palladium@Gold Core–Shell Nanocrystals with {431} High-Index Facets with Remarkable Electrochemiluminescence Activities. *ACS Nano., 8*(6), 5953-5958.

26. Wu, M. S., Qian, G. s., Xu, J. J. & Chen, H. Y. (2012). Sensitive Electrochemiluminescence Detection of c-Myc mRNA in Breast Cancer Cells on a Wireless Bipolar Electrode. *Analytical Chemistry, 84*(12), 5407-5414.

27. Qian, F., Wang, G. & Li, Y. (2010). Solar-Driven Microbial Photoelectrochemical Cells with a Nanowire Photocathode. *Nano Letters, 10*(11), 4686-4691.

28. Su, J., Guo, L., Bao, N. & Grimes, C. A. (2011). Nanostructured WO3/BiVO4 Heterojunction Films for Efficient Photoelectrochemical Water Splitting. *Nano Letters, 11*(5), 1928-1933.

29. Cheng, Y., Huang, Y., Lei, J., Zhang, L. & Ju, H. (2014). Design and Biosensing of Mg2+-Dependent DNAzyme-Triggered Ratiometric Electrochemiluminescence. *Analytical Chemistry, 86*(10), 5158-5163.

30. Wu, M. S., He, L. J., Xu, J. J. & Chen, H. Y. (2014). RuSi@Ru(bpy)$_3^{2+}$/Au@Ag_2S Nanoparticles Electrochemiluminescence Resonance Energy Transfer System for Sensitive DNA Detection. *Analytical Chemistry, 86*(9), 4559-4565.

31. Pandarinathan, V., Lepková, K. Bailey, S. I., Becker, T. & Gubner, R. (2014). Adsorption of Corrosion Inhibitor 1-Dodecylpyridinium Chloride on Carbon Steel Studied by in Situ AFM and Electrochemical Methods. *Industrial & Engineering Chemistry Research, 53*(14), 5858-5865.

32. Guo, Y., Jia, X. & Zhang, S. (2011). DNA cycle amplification device on magnetic microbeads for determination of thrombin based on graphene oxide enhancing signal-on electrochemiluminescence. *Chemical Communications, 47*(2), 725-727.

33. Chen, X., He, Y., Zhang, Y., Liu, M., Liu, Y. & Li, J. (2014). Ultrasensitive detection of cancer cells and glycan expression profiling based on a multivalent recognition and alkaline phosphatase-responsive electrogenerated chemiluminescence biosensor. *Nanoscale, 6*(19), 11196-11203.

34. Li, J., Hong, X., Li, D., Zhao, K., Wang, L., Wang, H., Du, Z., Li, J., Bai, Y. & Li, T. (2004). Mixed ligand system of cysteine and thioglycolic acid assisting in the synthesis of highly luminescent water-soluble CdTe nanorods. *Chemical Communications*, 1740-1741.

35. Wang, W., Hao, Q., Wang, W., Bao, L., Lei, J., Wang, Q. & Ju, H. (2014). Quantum dot-functionalized porous ZnO nanosheets as a visible light induced photoelectrochemical platform for DNA detection. *Nanoscale, 6*(5), 2710-2717.

36. Guo, Y., Sun, Y. & Zhang, S. (2011). Electrochemiluminescence induced photoelectrochemistry for sensing of the DNA based on DNA-linked CdS NPs superstructure with intercalator molecules. *Chemical Communications, 47*(5), 1595-1597.

37. Li, C., Lin, J., Guo, Y. & Zhang, S. (2011). A novel electrochemiluminescent reagent of cyclometalated iridium complex-based DNA biosensor and its application in cancer cell detection. *Chemical Communications, 47*(15), 4442-4444.

38. Zhang, X., Li, S., Jin, X. & Zhang, S. (2011). A new photoelectrochemical aptasensor for the detection of thrombin based on functionalized graphene and CdSe nanoparticles multilayers. *Chemical Communications, 47*, 4929-4931.

39. Gomez, B., Likhanova, N. V., Aguilar, M. A. D., Olivares, O., Hallen, J. M. & Martinez-Magadan, J. A. (2005). Theoretical study of a new group of corrosion inhibitors. *Journal of Physical Chemistry A., 109*(39), 8950-8957.

40. Kokalj, A. & Peljhan, S. (2010). Density Functional Theory Study of ATA, BTAH, and BTAOH as Copper Corrosion Inhibitors: Adsorption onto Cu(111) from Gas Phase. *Langmuir, 26*(18), 14582-14593.

41. Obi-Egbedi, N. O., Obot, I. B. & El-Khaiary, M. I. (2011). Quantum chemical investigation and statistical analysis of the relationship between corrosion inhibition efficiency and molecular structure of xanthene and its derivatives on mild steel in sulphuric acid. *Journal of Molecular Structure, 1002*(1-3), 86-96.

42. Radilla, J., Negrón-Silva, G. E., Palomar-Pardavé, M., Romero-Romo, M. & Galván, M. (2013). DFT study of the adsorption of the corrosion inhibitor 2-mercaptoimidazole onto Fe(100) surface. *Electrochimica Acta., 112*, 577-586.

43. Lashgari, M. (2011). Theoretical challenges in understanding the inhibition mechanism of aluminum corrosion in basic media in the presence of some p-phenol derivatives. *Electrochimica Acta., 56*(9), 3322-3327.

44. Hamani, H., Douadi, T., Al-Noaimi, M., Issaadi, S., Daoud, D. & Chafaa, S. (2014). Electrochemical and quantum chemical studies of some azomethine compounds as corrosion inhibitors for mild steel in 1M hydrochloric acid. *Corrosion Science, 88*.

45. Liu, A., Ren, X., Zhang, J., Wang, C., Yang, P., Zhang, J., An, M., Higgins, D., Li, Q. & Wu, G. (2014). Theoretical and Experimental Studies of the Corrosion Inhibition effect of Nitrotetrazolium Blue Chloride on Copper in 0.1 M H2SO4. *RSC Advances,* (76).

46. Nataraja, S. E., Venkatesha, T. V., Tandon, H. C. & Shylesha, B. S. (2011). Quantum chemical and experimental characterization of the effect of ziprasidone on the corrosion inhibition of steel in acid media. *Corrosion Science, 53*(12), 4109-4117.

47. Zhang, M., Yu, M., Li, F., Zhu, M., Li, M., Gao, Y., Li, L., Liu, Z., Zhang, J., Zhang, D., Yi, T. & Huang, C. (2007). A Highly Selective Fluorescence Turn-on Sensor for Cysteine/Homocysteine and Its Application in Bioimaging. *Journal of the American Chemical Society, 129*(34), 10322-10323.

48. Özcan, M. & Dehri, İ. (2004). Electrochemical and quantum chemical studies of some sulphur-containing organic compounds as inhibitors for the acid corrosion of mild steel. *Progress in Organic Coatings, 51*(3), 181-187.

49. Zong, X., Liang, M., Chen, T., Jia, J., Wang, L., Sun, Z. & Xue, S. (2012). Efficient iodine-free dye-sensitized solar cells employing truxene-based organic dyes. *Chemical Communications, 48*(53), 6645-6647.

50. Davies, M. L., Watson, T. M., Holliman, P. J., Connell, A. & Worsley, D. A. (2014). In situ monitoring and optimization of room temperature ultra-fast sensitization for dye-sensitized solar cells. *Chemical Communications, 50*(83), 12512-12514.

51. Lin, Z., Luo, F., Liu, Q., Chen, L., Qiu, B., Cai, Z. & Chen, G. (2011). Signal-on electrochemiluminescent biosensor for ATP based on the recombination of aptamer chip. *Chemical Communications, 47*(28), 8064-8066.

52. De Silva, S. S., Camp, P. J., Henderson, D. K., Henry, D. C. R., McNab, H., Tasker, P. A. & Wight, P. (2003). Attachment of phosphonate-functionalised azo-dyes to oxide surfaces to give enhanced light and wet fastness. *Chemical Communications,* (14), 1702-1703.

53. Zhang, H., Peng, J., Shen, Y., Yu, X., Zhang, F., Mei, J., Li, B. & Zhang, L. (2012). Hybrid microtubes of polyoxometalate and fluorescence dye with tunable photoluminescence. *Chemical Communications, 48*(37), 4462-4464.

54. Ali, M., Kumar, V. & Pandey, S. (2010). Unusual fluorescein prototropism within aqueous acidic 1-butyl-3-methylimidazolium tetrafluoroborate solution. *Chemical Communications, 46*(28), 5112-5114.

55. Egawa, T., Koide, Y., Hanaoka, K., Komatsu, T., Terai, T. & Nagano, T. (2011). Development of a fluorescein analogue, TokyoMagenta, as a novel scaffold for fluorescence probes in red region. *Chemical Communications, 47*(14), 4162-4164.

56. Emregül, K. C. & Atakol, O. (2003). Corrosion inhibition of mild steel with Schiff base compounds in 1 M HCl. *Materials Chemistry and Physics, 82*(1), 188-193.

57. Khalil, N. (2003). Quantum chemical approach of corrosion inhibition. *Electrochimica Acta., 48*(18), 2635-2640.

58. Bentiss, F., Traisnel, M., Vezin, H. & Lagrenée, M. (2003). Linear resistance model of the inhibition mechanism of steel in HCl by triazole and oxadiazole derivatives: structure-activity correlations. *Corrosion Science, 45*(2), 371-380.

59. Bastidas, J. M., Pinilla, P., Cano, E., Polo, J. L. & Miguel, S. (2003). Copper corrosion inhibition by triphenylmethane derivatives in sulphuric acid media. *Corrosion Science, 45*(2), 427-449.

60. Friseh, M. J., Schlegel, H. B. & Pople, J. A. (2003). Gaussian 03, Revi-sion A.1. , Gaussian Inc., Pittsburgh PA.

61. Zhang, X., Zhao, Y., Li, S. & Zhang, S. (2010). Photoelectrochemical biosensor for detection of adenosine triphosphate in the extracts of cancer cells. *Chemical Communications, 46*(48), 9173-9175.

62. Guo, H., Ji, S., Wu, W., Wu, W., Shao, J. & Zhao, J. (2010). Long-lived emissive intra-ligand triplet excited states (3IL): next generation luminescent oxygen sensing scheme and a case study with red phosphorescent diimine Pt(ii) bis(acetylide) complexes containing ethynylated naphthalimide or pyrene subunits. *Analyst, 135*(11), 2832-2840.

63. Zhao, J. & James, T. D. (2005). Enhanced fluorescence and chiral discrimination for tartaric acid in a dual fluorophore boronic acid receptor. *Chemical Communications,* (14), 1889-1891.

64. Zhao, J. & James, T. D. (2005). Chemoselective and enantioselective fluorescent recognition of sugar alcohols by a bisboronic acid receptor. *Journal of Materials Chemistry, 15*(27-28), 2896-2901.

65. Mansfeld, F., Kendig, M. W. & Tsai, S. (1982). Recording and Analysis of AC Impedance Data for Corrosion Studies. *Corrosion, 37*(5), 570-580.

66. Cruz, J., Martínez, R., Genesca, J. & García-Ochoa, E. (2004). Experimental and theoretical study of 1-(2-ethylamino)-2-methylimidazoline as an inhibitor of carbon steel corrosion in acid media. *Journal of Electroanalytical Chemistry, 566*(1), 111-121.

67. Hosseini, M., Mertens, S. F. L., Ghorbani, M. & Arshadi, M. R. (2003). Asymmetrical Schiff bases as inhibitors of mild steel corrosion in sulphuric acid media. *Materials Chemistry and Physics, 78*(3), 800-808.

68. McCafferty, E. & Hackerman, N. (1972). Double Layer Capacitance of Iron and Corrosion Inhibition with Polymethylene Diamines. *Journal of The Electrochemical Society, 119*(2), 146-154.

69. Tang, L., Mu, G. & Liu, G. (2003). The effect of neutral red on the corrosion inhibition of cold rolled steel in 1.0 M hydrochloric acid. *Corrosion Science, 45*(10), 2251-2262.

70. Li, X., Tang, L., Li, L., Mu, G. & Liu, G. (2006). Synergistic inhibition between o-phenanthroline and chloride ion for steel corrosion in sulphuric acid. *Corrosion Science, 48*(2), 308-321.